THE JOURNAL OF PHYSICAL CHEMISTRY A

Article

pubs.acs.org/JPCA

Radiation Products at 77 K in Trehalose Single Crystals: EMR and DFT Analysis

Mihaela Adeluta Tarpan,[†] Hendrik De Cooman,[†,‡] Eli Olaug Hole,[§] Michel Waroquier,[‡] and Freddy Callens*[,†]

[†]Department of Solid State Sciences, Ghent University, Krijgslaan 281-S1, B-9000 Gent, Belgium

[‡]Center for Molecular Modeling, Ghent University, Technologiepark 903, B-9052 Zwijnaarde, Belgium

[§]Department of Physics, University of Oslo, P.O. Box 1048 Blindern, N-0316 Oslo, Norway

Supporting Information

ABSTRACT: The radicals obtained in trehalose dihydrate single crystals after 77 K X-irradiation have been investigated at the same temperature using X-band electron paramagnetic resonance (EPR), electron nuclear double resonance (ENDOR), and ENDOR-induced EPR (EIE) techniques. Five proton hyperfine coupling tensors were unambiguously determined from the ENDOR measurements and assigned to three carbon-centered radical species (T1, T1*, and T2) based on the EIE spectra. EPR angular variations revealed the presence of four additional alkoxy radical species (T3 to T6) and allowed determination of their g tensors. Using periodic density functional theory (DFT) calculations, T1/T1*, T2, and T3 were identified as H-loss species centered at C4, C1′, and O2′, respectively. The T4 radical is proposed to have the unpaired electron at O4, but considerable discrepancies between experimental and calculated HFC values indicate it is not simply the (net) H-loss species. No suitable models were found for T5 and T6. These exhibit a markedly larger g anisotropy than T3 and T4, which were not reproduced by any of our DFT calculations.

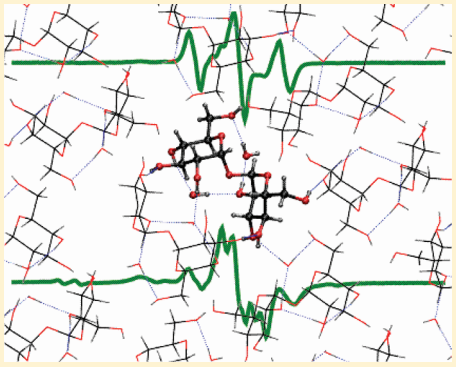

1. INTRODUCTION

Numerous electron paramagnetic resonance (EPR) studies have been performed on radiation-induced free radicals in carbohydrates in the last decades. Motivations for studying this type of systems include dosimetric applications,[1−4] a better understanding of the consequences of radiation treatment of different sugar-containing foodstuffs,[5−7] and increased insight in the radiation chemistry of more complex, carbohydrate-containing biomolecules like DNA.[8−12] In spite of their apparent simplicity, carbohydrates exhibit a remarkably complex radiation chemistry and investigating the radiation-induced radical structures and reaction mechanisms in these compounds is relevant in elucidating phenomena of fundamental importance, like radiation regioselectivity (i.e., the tendency of radiation to inflict damage preferentially at certain sites in a molecule).

Reliable identification of radiation-induced radicals and reactions in molecular solids is a challenging task and usually requires a combined experimental/theoretical approach. Electron magnetic resonance (EMR) measurements (EPR, electron nuclear double resonance (ENDOR) and ENDOR-induced EPR (EIE)) allow detailed characterization of radical structures, while advanced, periodic density functional theory (DFT) calculations of spin Hamiltonian parameters, primarily proton hyperfine coupling (HFC) tensors, on geometry-optimized radical structures provide an accurate and reliable way of identifying these structures (see, e.g., sucrose,[13−15] fructose,[16,17] rhamnose,[18−20] and glucose-1-phosphate[21,22]). Primary radicals and transformation mechanisms leading to the final stable products can be studied by investigating the radiation products obtained by irradiation at low (10 K) and intermediate temperatures (e.g., 77 K).

In this study, we apply this combined EMR/DFT methodology to characterize and identify the major radicals present in X-irradiated trehalose dihydrate single crystals (Figure 1) after

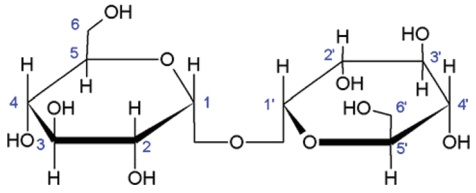

Figure 1. Chemical structure and atom numbering of trehalose.

77 K irradiation. This is a continuation of a previous study of the radicals after 10 K irradiation, recently published by our group.[23]

X-irradiated trehalose single crystals have been the subject of a number of EMR studies. In Table 1, a summary of results

Received: January 31, 2012
Revised: March 5, 2012
Published: March 5, 2012

   dx.doi.org/10.1021/jp300979g | J. Phys. Chem. A 2012, 116, 3377−3387

Table 1. Summary of Literature Results on Radical Species Obtained after X-Irradiation at Various Temperatures in Trehalose Dihydrate Single Crystals As Well As Those Obtained in the Present Study[a]

radical type	3 K[24]		10 K[23]		77 K (present study)		77 K[25]
trapped electron	radical I		not observed		not observed		not observed
alkyl radicals	radical II	(=)	R1 (C5′)	≠	T1/T1* (C4)	=	radical VII
			R2 (C5)	=	R2 (C5)	=	radical VI
					T2 (C1′)		
alkoxy radicals	radical III	=	R3 (O2)	=	R3 (O2)	=	radical II
			R4 (O4′)				
			T3 (O2′)	=	T3 (O2′)		
					T4 (O4?)	=	radical I
					T5	=	radical III
			T6	=	T6	(=)	radical IV

[a]The carbon or oxygen atom between parentheses is the radical center identified using DFT calculations. An equality sign between parentheses indicates that the correspondence is likely but not certain.

obtained after X-irradiation at various temperatures below room temperature (RT) (3 K,[24] 10 K,[23] and 77 K[25]) is presented together with the results obtained in the present study.

Samskog et al.[24] reported the presence of three different radicals after 3 K X-irradiation: a trapped electron (radical I), an alkyl radical (radical II), and an alkoxy radical (radical III). Radicals II and III were proposed to be H-loss species centered at either C3 or C3′ (radical II) and O4′ (radical III), respectively. (Note that the terms alkyl and alkoxy are not used in the strict sense throughout this work but rather indicate whether the radical is carbon- or oxygen-centered, as is often done in related literature.)

Very recently, we investigated the species obtained after 10 K irradiation in our laboratories.[23] ENDOR and EIE, which were not employed by Samskog et al., together with advanced periodic DFT calculations, allowed identification of two alkyl (R1, R2) and two alkoxy (R3, R4) radical species. R2 and R3 had not been reported in the 3 K study by Samskog et al.[24] and were identified as H-loss C5- and O2-centered radicals, respectively. R1 most likely corresponds to radical II in the 3 K study as both exhibit a 1:2:1 triplet EPR line pattern with a 3 mT hyperfine splitting. However, our DFT calculations convincingly identified the radical center as C5′, and not C3 or C3′. R4 corresponds to radical III, as testified by a good agreement between the experimental EPR angular variations of R4 at 10 K with simulations using the g tensor of radical III. In this case, our DFT calculations confirm the assignation to an O4′-centered alkoxy radical. The absence of the EPR signal of radical I (the trapped electron) observed at 3 K and reported to be stable up to 50 K by Samskog et al.,[24] in both the EPR and ENDOR spectra at 10 K is remarkable. We have reported on a similar discrepancy for sucrose single crystals.[15]

In another study conducted by Samskog and Kispert, this time at 77 K, four different alkoxy radicals (I to IV) and two alkyl radicals (VI and VII) were observed.[25] The authors suggested species I, II, III, VI ,and VII to result from net H loss at O2′, O2, O3′, C2, and C3 or C3′, respectively. Radical species IV was proposed to be an anion with the main site of spin density at the ring oxygen O5. When the crystal was stored at 77 K for two weeks, radical II decayed with the concomitant growth of a new alkyl radical (V), supposedly C6-centered. Radical VII exhibited a 1:2:1 triplet EPR pattern with a 3 mT hyperfine splitting very similar to that of radical II at 3 K (and also radical R1 at 10 K), and Samskog and Kispert assumed these to be chemically identical species.

Previous studies in our lab (e.g., on the radicals in trehalose after 10 K irradiation[23,24] and the stable radicals in sucrose[13−15,26]) have clearly demonstrated that the more advanced EMR techniques and DFT calculations available today allow for a considerably more complete and accurate analysis than is possible by EPR alone. Therefore, reinvestigations of this type of systems with modern-day tools is important in order to establish a reliable framework for understanding radiation damage to organic materials and sugars in particular. The present study is a reinvestigation of the radicals obtained after in situ 77 K X-irradiation in trehalose dihydrate single crystals.

2. MATERIALS AND METHODS

The crystal structure of trehalose dihydrate is orthorhombic ($P2_12_12_1$) and contains four molecules $C_{12}H_{22}O_{11}\cdot 2H_2O$ in a unit cell.[27] The crystal axes were chosen as the reference frame for the EPR, ENDOR, and EIE measurements. The procedures for growth of single crystals, sample orientation, and X-band EPR/ENDOR/EIE measurements, after in situ X-irradiation at low temperature using the home-built setup at the University of Oslo, have been described previously.[16,23] A Philips chromium-anode X-ray tube operated at 60 kV and 40 mA was used for the irradiation, and an estimated dose of about 45 kGy was delivered to the crystal at a typical dose rate of 0.5 kGy per minute.

The EPR and ENDOR measurements were performed in the ab, ac, and bc planes, as well as in a skewed plane (θ = 30°; φ = 90°; θ and φ being the usual polar angles). The spectra were recorded every 5° over at least 90° in each plane. ENDOR spectra were obtained at several magnetic field values for every orientation. Proton HFC tensors were determined from the ENDOR angular variations with the program MAGRES.[28] The skewed plane results allowed choosing the correct Schonland form.[29,30] EPR spectra were in general recorded for two different microwave powers (0.01 mW and 10 mW). The various ENDOR lines were assigned to particular radical species with the aid of EIE measurements along the ⟨a⟩, ⟨b⟩, and ⟨c⟩ axes. For the determination of the g tensors, the simulations of EPR and EIE spectra and of the ENDOR angular variations, the EasySpin[31] routines in Matlab were used.

3. COMPUTATIONAL DETAILS

The same computational protocol as in ref 23 was used: all calculations were performed in a DFT framework, with a BLYP functional[32,33] and using the CP2K program package,[34] on a

crystal unit cell (four trehalose and eight water molecules) with periodic boundary conditions. All-electron geometry optimizations, HFC tensor[35] and g tensor[36] calculations, were done using the Gaussian-augmented plane-wave (GAPW) method[37] (plane-wave cutoff of 250 Ry, TZV2P basis set). The former were often preceded by pseudopotential calculations in the Gaussian and plane-waves (GPW) approach[38] (plane-wave cutoff of 320 Ry, TZV2P GTH basis sets,[39] GTH pseudopotentials[40,41]) to increase computational efficiency.

When DFT-calculated and experimental eigenvectors or crystal directions are compared, symmetry operations are performed on the experimental eigenvectors to obtain the best possible agreement (i.e., the smallest deviation angle).

4. EXPERIMENTAL RESULTS AND RADICAL MODEL ASSIGNMENT

4.1. Temperature Dependence. Figure 2 shows intensity-normalized X-band EPR spectra recorded along the ⟨c⟩ axis

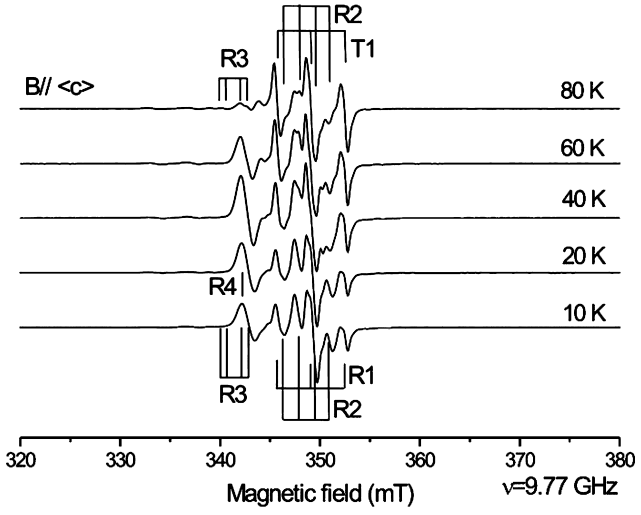

Figure 2. Temperature dependence of the EPR spectrum of a trehalose single crystal X-irradiated at 10 K, recorded with the magnetic field along ⟨c⟩. All spectra are normalized to a microwave frequency of 9.77 GHz and recorded at 10 K. The annealing temperature is given at the right-hand side. Details of the annealing procedure are given in the text. The stick diagrams outline the hyperfine patterns, based on the ENDOR data and the EPR angular variations.

after annealing to various temperatures. The sample was in situ X-irradiated at 10 K, annealed at the desired temperature (20 K, 40 K, 60 K, and 80 K) for half an hour after temperature stabilization, and then cooled back down to 10 K for the measurement. The 10 K spectrum was recorded before any annealing was carried out.

Complementary experiments showed that the EPR spectra of trehalose single crystals irradiated at 77 K are very similar to those obtained after irradiation at 10 K and annealing to 80 K (Figure 3). The minor discrepancies in the positions of the weaker lines are most probably due to the difference in measuring temperature and/or a small difference in orientation.

Annealing to 80 K induces substantial changes in the EPR spectrum, the most obvious one being the complete decay of alkoxy radical R4, which appears to be relatively stable up to 60 K. A 1:2:1 triplet with a 3 mT hyperfine splitting is apparent in all spectra, regardless of the annealing temperature, and

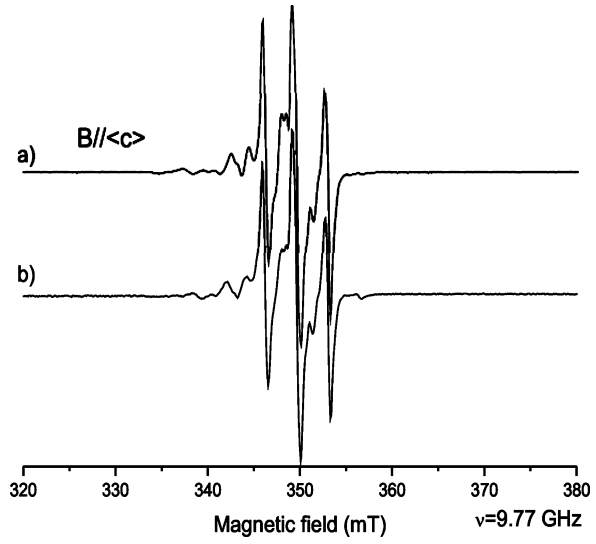

Figure 3. X-band EPR spectra recorded with the magnetic field along ⟨c⟩ for a trehalose single crystal (a) X-irradiated at 10 K, annealed at 80 K and measured at 10 K (this corresponds to the 80 K spectrum in Figure 2) and (b) X-irradiated and measured at 77 K. The spectra were recorded with a microwave power of 0.01 mW and were normalized to a microwave frequency of 9.77 GHz.

dominates the 80 K spectrum. At 10 K, this triplet corresponds to radical R1, which was earlier identified as a hydrogen-loss C5′-centered radical.[23] The nature of the 80 K triplet, labeled T1, will be discussed in detail in section 4.3.

EPR and ENDOR angular variations showed that two of the radicals obtained after 10 K irradiation, alkyl radical R2 and alkoxy radical R3, are still present after annealing of the sample to 80 K. Moreover, the EPR lines corresponding to R3 are better visible at 80 K for some particular orientations (as for B//⟨c⟩ in Figure 2) due to the decay of R4.

4.2. Experimental EPR, ENDOR, and EIE Results. All EPR, ENDOR, and EIE measurements presented in this section were carried out at 77 K after in situ X-irradiation at 77 K without annealing of the sample in between. In Figure 4, typical

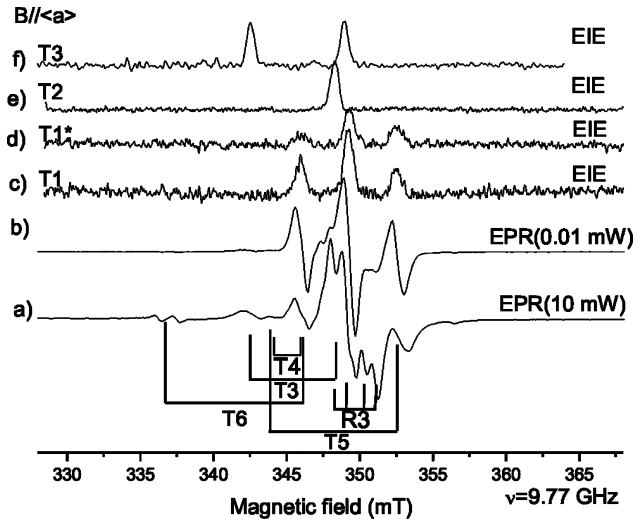

Figure 4. X-band EPR spectra at 77 K for 10 mW (a) and 0.01 mW (b) microwave power, and EIE spectra (c to f) of trehalose single crystals X-irradiated at 77 K, all recorded with the magnetic field along ⟨a⟩. The stick diagrams outline the hyperfine patterns, based on the ENDOR data and the EPR angular variations.

dx.doi.org/10.1021/jp300979g | J. Phys. Chem. A 2012, 116, 3377−3387

X-band EPR spectra for 10 mW (Figure 4a) and 0.01 mW (Figure 4b) microwave power for the magnetic field along the ⟨a⟩ axis are shown. EPR angular variations reveal both centers with small and relatively large g anisotropy, indicating the presence of both alkyl and alkoxy radicals, respectively.[42,43] Because of the differences in relaxation times and hence power-saturation behavior, the alkoxy radicals are better visible at high microwave power (10 mW), whereas the alkyl radicals are preferably measured at low microwave power (0.01 mW).

4.2.1. Alkoxy Radicals (R3 and T3−T6). As mentioned above, alkoxy species R3 is also present after 10 K irradiation, and it has been analyzed and identified as an H-loss, O2-centered alkoxy radical in a previous study in our laboratories.[23] It was reported for the first time at 10 K in that study, but it corresponds to species II observed at 77 K in the study by Samskog and Kispert:[25] the g tensor principal values agree well, the g tensor principal directions deviate by less than 4°, and both species have two HFCs with comparable magnitudes and anisotropy. Samskog and Kispert also assigned this species to an alkoxy radical centered at O2. It dominates the EPR spectrum at high microwave power (Figure 4a), which indicates that it is the alkoxy species with the (by far) highest relative concentration at 77 K.

The g tensors of alkoxy radicals T3 and T4 (Table 2) were obtained from EPR angular variations at higher microwave power (10 mW) (Figure 5) by extracting the effective g factor of a radical for a particular orientation from the center of the hyperfine pattern. An EIE spectrum assigned to T3 was obtained off one of the unassigned ENDOR lines very close to the proton Larmor frequency (labeled HF2(T3) in Figure 6) for the magnetic field along ⟨a⟩. The doublet structure of this EIE spectrum (labeled T3 in Figures 4a and 4f) has a hyperfine

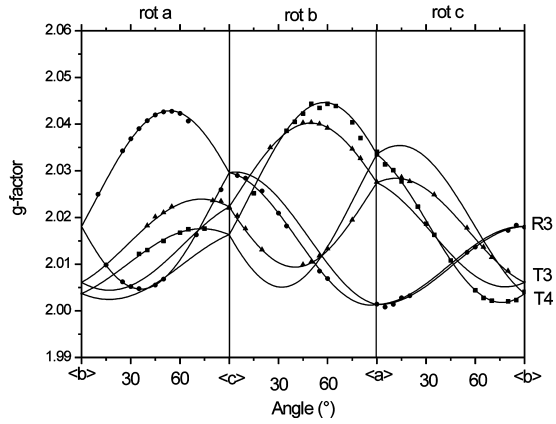

Figure 5. Experimental angular dependence of the g factor of alkoxy radical species R3 (solid circles), T3 (triangles), and T4 (squares), and simulations (solid lines) using the g tensors in ref 23 (R3) and in Table 2 (T3 and T4).

splitting of approximately 6.5 mT (180 MHz). We have not been able to determine any of the HFC tensors associated to T3 in a reliable way; neither for the small HF2(T3) hyperfine interaction (which is only 4 MHz for B//⟨a⟩ and may originate from a proton in a β or a more distant position) nor from the large, relatively isotropic β-type HFC of approximately 6.5 mT. Radical T4 is characterized by an EPR hyperfine doublet (labeled T4 in Figure 4a) with a rather isotropic splitting of approximately 2 mT. The corresponding HFC tensor could again not reliably be determined from the EPR spectra.

The EPR signatures of radicals T5 and T6 could be observed at sufficient orientations (for a clear angular variation pattern to

Table 2. Experimental Proton HFC Tensors (in MHz) Obtained from X-Band ENDOR Angular Variations at 77 K for Radicals T1, T1*, and T2, and Experimental g Tensors and Estimated HFC Values Obtained from EPR Angular Variations at 77 K for Radicals T3 and T4

					principal directions		
radical	tensor	principal values	isotropic value	anisotropic values	a	b	c
T1	HF1(T1)	105.36	98.67	6.69	−0.054	0.722	0.69
		97.72		−0.95	0.189	−0.686	0.703
		92.94		−5.73	−0.981	−0.093	−0.173
	HF2(T1)	97.56	90.18	7.38	0.641	0.353	−0.682
		87.66		−2.52	0.643	−0.732	0.225
		85.33		−4.85	0.419	0.583	0.696
T1*	HF1(T1*)	103.27	96.63	6.65	−0.142	0.735	0.663
		95.33		−1.3	0.121	−0.677	0.726
		91.28		−5.35	−0.982	−0.023	−0.185
	HF2(T1*)	94.89	87.07	7.82	0.653	0.395	−0.646
		83.57		−3.51	0.675	−0.691	0.26
		82.76		−4.31	0.343	0.605	0.718
T2	HF1(T2)	18.9	9.4	9.49	0.226	0.906	−0.357
		5.2		−4.21	−0.362	0.418	0.833
		4.12		−5.29	0.905	0.059	0.422
T3	g(T3)	2.0421			0.765	0.026	0.644
		2.0169			−0.491	0.624	0.608
		2.0022			0.418	0.781	−0.465
	HF1	∼180					
	HF2	<7					
T4	g(T4)	2.0483			0.831	−0.202	0.518
		2.0070			−0.49	0.175	0.854
		2.0036			0.263	0.964	−0.046
	HF1	∼56					

dx.doi.org/10.1021/jp300979g | J. Phys. Chem. A 2012, 116, 3377−3387

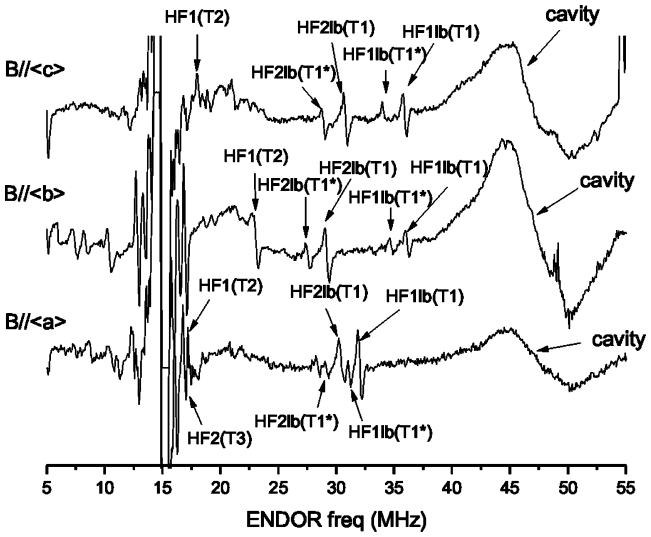

Figure 6. X-band ENDOR spectra at 77 K of trehalose single crystals X-irradiated at 77 K for the magnetic field along ⟨a⟩, ⟨b⟩, and ⟨c⟩. The magnetic field was locked each time at the central line of the dominating triplet in the EPR spectrum. Because of the experimental problems, only the low-frequency ENDOR branches could be recorded for T1 and T1* radicals, and they were marked with "lb" in their labels. The broad feature at 40−55 MHz (denoted cavity) is generated by a background detector dc-shift.

be visible) in only two rotation planes in the present study: T5 in bc and ab and T6 in ab and ac. Both radicals are characterized by doublet EPR spectra, with a relatively isotropic splitting of approximately 9 mT. These species appear to correspond to radicals III and IV in the 77 K study by Samskog and Kispert.[25] This conclusion is based on the close correspondence between our experimental EPR angular variations for T5 and T6 and the EPR angular variations for their radicals III and IV, which were simulated using their reported g tensors and estimated HFC values (ref 25, reproduced in Table 3 of the current work). The comparison is presented in Figure S1 in the Supporting Information.

Table 3. Experimental g Tensors and Estimated HFC Values (in mT) for the Alkoxy Radicals III and IV in Trehalose Single Crystals Irradiated at 77 K, Determined from X-Band EPR Angular Variations at 77 K, As Reported by Samskog and Kispert[25] (These Correspond to Radical Species T5 and T6, Respectively, in the Current Study)

			principal directions		
radical	tensor	principal values	a	b	c
T5 (radical III)	g	2.0836	−0.326	0.904	−0.277
		2.0052	−0.376	−0.393	−0.839
		2.0015	0.868	0.169	−0.467
	HF1	9.0−9.5			
T6 (radical IV)	g	2.0865	0.745	0.033	0.666
		2.0068	−0.351	0.868	0.350
		1.9991	−0.567	−0.495	0.658
	HF1	9.0−9.5			
	HF2	<0.6			

Careful comparison of the EPR angular variations recorded after irradiation at 10 K[23] and 77 K shows that radicals T3 and T6 are present at both temperatures. In the 10 K study, these lines could not be assigned, and the corresponding g tensors or HFC tensors were not obtained because they were not resolved for a sufficient number of orientations. The relative intensity of their EPR lines is quite small, even at high microwave power, at 77 K as well.

4.2.2. Alkyl Radicals (R2, T1, T1, and T2).* Like R3, alkyl species R2 is also present after 10 K irradiation and has been analyzed at 10 K in a previous study.[23] A number of relatively intense lines due to other alkyl radicals were observed in the ENDOR spectra recorded on the portion of the EPR spectrum around g ≈ 2 (Figure 6). Angular variations allowed the determination of five HFC tensors (Table 2), although more couplings are evident from the ENDOR spectra. In Figure 7,

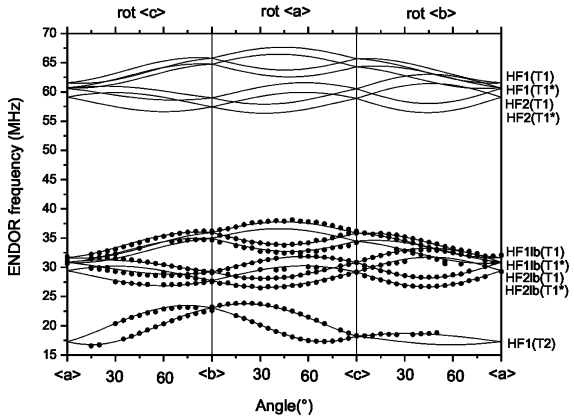

Figure 7. ENDOR angular variation in the ab, bc, and ca planes for the T1, T1*, and T2 proton HFC interactions. The solid circles represent experimental resonance positions, and the solid lines are simulations using the HFC tensors in Table 2. The simulations for both the low- and high-frequency branches corresponding to T1 and T1* are presented.

the angular dependences of the assigned ENDOR lines are shown. Because of the technical problems, ENDOR spectra could not be recorded above 55 MHz, and the low-frequency branches were used for determining the HFC tensors of HF1(T1), HF1(T1*), HF2(T1), and HF2(T1*).

EIE analysis at several orientations showed that the five proton HFC interactions can be attributed to three radicals: T1, T1*, and T2. In Figure 4, the corresponding EIE spectra are shown for the magnetic field along ⟨a⟩. T1 and T1* each exhibit two large β-type proton HFCs with isotropic values around 90−100 MHz (Table 2 and Figure 4c,d, respectively). The similarity of the HFC tensors suggests that these radicals are the same chemical species stabilized in two slightly different geometrical conformations, as often occurs in this type of crystals.[13,16,44] Figure 4b clearly shows T1/T1* is the most abundant alkyl radical as its triplet signal dominates the EPR spectrum at lower microwave power. In accordance with the rather narrow EIE singlet of T2 (Figure 4e), only one small and fairly isotropic HFC was assigned to this species (HF1(T2) in Table 2). The principal values of the corresponding tensor again are typical of a β-proton interaction.

4.3. Radical Model Assignment. X-irradiation of trehalose single crystals at 77 K results in the formation of at least nine radical species: T1, T1*, T2−T6, R2, and R3. R2 and R3 have already been identified in a previous study as an H-loss alkyl radical centered at C5 and an H-loss alkoxy radical centered at O2, respectively.[23] In this section, models for the other seven species are discussed. In view of the low temperature used for the in situ irradiation, structures obtained by

dx.doi.org/10.1021/jp300979g | J. Phys. Chem. A 2012, 116, 3377−3387

Table 4. DFT-Calculated Proton HFC Tensor (in MHz) for an H-Loss C4-Centered Radical Species (M1 in Figure 8)[a]

				principal directions						
radical model	proton	isotropic value	anisotropic value	a	b	c	δ1 (deg)	δ1′ (deg)	δ2 (deg)	δ2′ (deg)
M1	H(C3)	84.03	6.79	−0.121	0.717	0.686	4		2	
			−0.95	0.076	−0.682	0.727	7		3	
			−5.83	−0.99	−0.141	−0.028	9		11	
	H(C5)	80.48	7.21	0.577	0.414	−0.704		5		6
			−2.97	0.779	−0.539	0.322		15		11
			−4.24	0.246	0.734	0.633		14		10
	H(O4)	−2.42	−10.56	0.306	0.654	0.692				
			−8.84	0.216	−0.755	0.619				
			19.4	−0.927	0.04	0.372				

[a] δ1, δ1′, δ2, and δ2′ represent the angles between the DFT-calculated and experimental principal directions of HF1(T1), HF2(T1), HF1(T1*), and HF2(T1*) (Table 2), respectively.

simple alterations to the pristine molecule, such as net hydrogen loss, were investigated first. It will be shown that radicals T1/T1*, T2, and T3 indeed are such species.

*4.3.1. Alkyl Radical T1/T1**. T1/T1* is an alkyl radical with two roughly equally big β-type HFCs of 85−100 MHz, and its EPR spectrum exhibits the same general features (a 1:2:1 triplet with a splitting of roughly 3 mT) as the alkyl radical VII reported in the 77 K irradiation study by Samskog and Kispert.[25]

Hydrogen loss at C2, C3, C4, C5, C2′, C3′, C4′, and C5′ may in principle result in a radical with these features. Comparison of crystallographic $C_\alpha-H_\beta$ directions with the experimental A_{max} eigenvectors for the four HFCs assigned to T1/T1* (Table S1 in Supporting Information) favors C3 and C4 (deviations of less than 20° for both couplings), and C5 and C5′ cannot be ruled out (small deviation of 12° or less for one coupling, a larger deviation of at least 26° for the other). C2′ and C4′, and definitely C2 and C3′, are (much) less likely candidates as the deviations are markedly larger.

The DFT calculated proton HFC tensors for those four H-loss species (centered at C3, C4, C5, and C5′) are reported and compared with the experimental ones in Table S2 in the Supporting Information. In Table 4, the results are shown for the C4-centered species (model M1 in Figure 8), which is the

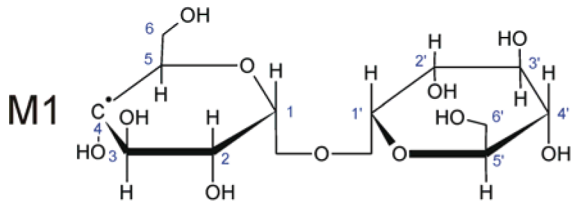

Figure 8. Chemical structure radical model M1 (DFT calculations are reported in Table 4).

only one that shows satisfactory agreement with respect to principal values and directions for both couplings. The H(C3) and H(C5) protons correspond to HF1(T1)/HF1(T1*) and HF2(T1)/HF2(T1*), respectively. The HFC to the H(O4) hydroxy proton is predicted to have a negligible isotropic component, also in agreement with experimental observations. For the other species, much larger discrepancies are found. Most notably, the C5-centered species has only one large HFC, and the C3-, C5-, and C5′-centered species all show large deviations in principal directions. We therefore assign T1/T1* to a C4-centered hydroxyalkyl radical.

4.3.2. Alkyl Radical T2. T2 is an alkyl radical with only one significant HFC, which has an anisotropy typical for a β-proton interaction and a small isotropic value of approximately 9 MHz (Table 2). This trehalose radical species has not been reported previously.

Considering only H loss events, the radical species centered at C1 or C1′ (M2 and M3, respectively, in Figure 9) are a

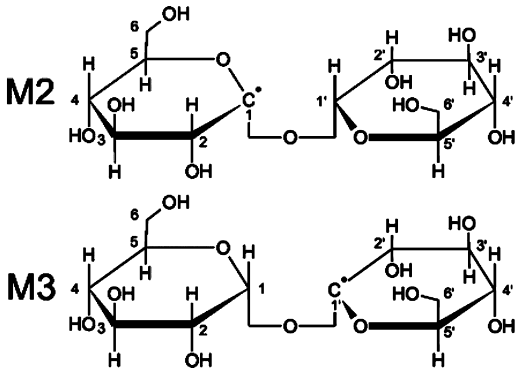

Figure 9. Chemical structures of radical models M2 and M3 (DFT calculations are reported in Table 5).

priori most likely to show only one small β-HFC, as the radical centers are neighbored by both a ring oxygen and the glycosidic oxygen. DFT-calculated HFC tensors for these radical structures are given in Table 5. The β-proton HFC tensor matches the experimental data equally well with respect to principal values for both species, a difference of 10−15 MHz in isotropic HFC being within the typical accuracy for this type of calculation.[45] The principal directions of M3 agree substantially better with the experimental ones, however, with deviations of about 10°. We therefore propose that radical species T2 results from net H-loss at C1′.

4.3.3. Alkoxy Radical T3. T3 is an alkoxy radical (as is evident from the g anisotropy) reported for the first time in the present study. It has a relatively isotropic HFC of about 180 MHz and at least one much smaller HFC (observed maximum less than 7 MHz). The associated g tensor is given in Table 2, but no HFC tensors could be determined (section 4.2.1). Comparing the g_{max} eigenvector, which is nearly parallel with the C−O• bond for an alkoxy radical, with all C−O bond directions in the pristine molecule (Table S3 in Supporting Information), the most plausible sites for the unpaired electron are found to be O3, O4, and O2′. Table 6 presents the DFT-calculated HFC tensors and g tensors of the corresponding alkoxy species (M4, M5, and M6 in Figure 10).

dx.doi.org/10.1021/jp300979g | J. Phys. Chem. A 2012, 116, 3377−3387

Table 5. DFT-Calculated Proton HFC Tensors (in MHz) for H-Loss Radical Species Centered at C1 and C1′ (M2 and M3 in Figure 9, Respectively)[a]

				principal directions			
radical model	proton	isotropic value	anisotropic value	a	b	c	δ (deg)
M2	H(C2)	19.15	10.41	0.380	0.724	−0.575	19
			−4.63	0.878	−0.088	0.470	42
			−5.77	−0.289	0.684	0.670	54
M3	H(C2′)	23.78	10.51	0.062	0.913	−0.403	9
			−4.21	−0.226	0.406	0.885	8
			−6.30	0.972	0.036	0.232	11

[a] δ represents the angle between the DFT-calculated and experimental principal directions of HF1(T2) (Table 2).

Table 6. DFT-Calculated Proton HFC Tensors (in MHz) and g Tensors of H-Loss Radical Species Centered at O3, O4, and O2′ (Models M4, M5, and M6 in Figure 10, Respectively)[a]

					principal directions			δ (deg)	
radical model	tensor	principal values	isotropic value	anisotropic values	a	b	c	T3	T4
M4	H(C3)	113.65	103.42	10.23	0.05	0.836	−0.546		
		98.84		−4.57	0.958	0.114	0.262		
		97.76		−5.66	−0.281	0.537	0.796		
	H(C4)	8.87	0.99	7.88	0.208	−0.863	−0.46		
		1.65		0.65	−0.269	−0.503	0.821		
		−7.54		−8.53	0.94	0.046	0.337		
	g	2.0367			−0.668	−0.564	0.486	33	23
		2.0098			−0.737	0.409	−0.539	19	41
		2.0029			0.105	−0.718	−0.688	33	47
M5	H(C3)	3.9	−2.68	6.58	0.177	0.685	0.707		
		−3.62		−0.95	−0.475	0.688	−0.548		
		−8.31		−5.64	−0.862	−0.239	0.447		
	H(C4)	264.42	252.19	12.23	−0.264	0.885	−0.383		
		248.26		−3.92	0.867	0.392	0.309		
		243.87		−8.31	−0.423	0.251	0.871		
	H(C5)	9.25	3.09	6.16	0.851	0.33	−0.409		
		0.57		−2.52	0.51	−0.336	0.792		
		−0.56		−3.64	−0.123	0.882	0.454		
	g	2.0466			0.804	−0.271	0.529	18	4
		2.0093			−0.546	0.015	0.838	38	10
		2.0032			0.235	0.963	0.135	38	10
M6	H(C2′)	217.34	206.64	10.7	−0.916	−0.345	0.206		
		203.93		−2.7	−0.264	0.13	−0.956		
		198.64		−8	−0.303	0.93	0.21		
	H(water)	17.37	−0.7	18.07	−0.198	−0.387	−0.9		
		−8.52		−7.82	−0.549	−0.717	0.429		
		−10.95		−10.25	−0.812	0.58	−0.07		
	g	2.0457			0.804	0.112	0.584	9	18
		2.0103			−0.532	0.575	0.621	4	27
		2.0048			0.266	0.81	−0.522	7	29

[a] δ represents the angle between the DFT-calculated and experimental g tensor principal directions (Table 2).

As previous studies[15,19,23] indicate that the DFT-calculated g tensor principal *values* are not accurate enough to discriminate between such similar values as given in Table 6, the g tensor principal *directions* are considered as primary criterion for distinguishing between the various models. In this respect, M6 matches the experimental data well (deviations of less than 10° for all g tensor principal directions) and significantly better than M4 and M5. Also, two HFC interactions with the right magnitude are predicted, one small coupling to a proton from a neighboring water molecule hydrogen-bound to O2′ and one large coupling to H(C2′) (isotropic value of about 200 MHz).

Accurate determination of the experimental HFC tensors would allow a more rigorous identification, but the good correlation between all available experimental data and the DFT calculations strongly suggests that T3 is an H-loss, O2′-centered species (M6 in Figure 10).

4.3.4. Alkoxy Radical T4. T4 also exhibits a g anisotropy typical of an alkoxy radical (Table 2). The EPR-spectra are characterized by a rather isotropic doublet splitting of approximately 2 mT (56 MHz), indicative of a coupling to a β-proton, although more remote protons cannot be discarded. (For example, a δ-proton HFC of 67 MHz has been observed in a rhamnose alkoxy species.[19,46] This radical corresponds well to species I in the 77 K study by Samskog and Kispert,[25] both in g tensor principal values and directions (deviations of 5° or less) and in hyperfine pattern (both exhibit one HFC of comparable

dx.doi.org/10.1021/jp300979g | J. Phys. Chem. A 2012, 116, 3377−3387

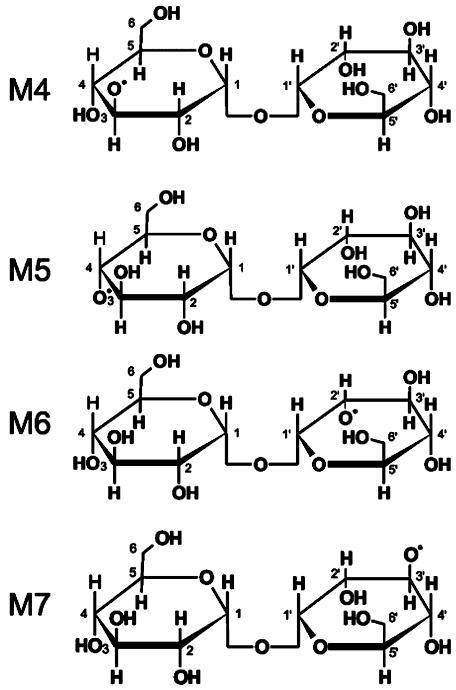

Figure 10. Chemical structures of radical models M4−M7 (DFT calculations are reported in Table 6).

magnitude). Samskog and Kispert assigned species I to an O2′-centered (H-loss) alkoxy radical. Comparing the pristine C−O bond directions with the experimental g_{max} principal value, O3, O4, and O2′ appear to be the most plausible sites for the unpaired electron (see Table S3, Supporting Information), as was the case for radical T3. Table 6 presents the DFT-calculated tensors (HFC and g) of the corresponding alkoxy species (M4, M5, and M6, respectively, Figure 10).

Again relying in first instance on the g tensor principal *directions*, model M5 (O4-centered) fits best with the experimental observations, with a maximum deviation of 10°. However, the DFT calculation predicts a much larger isotropic HFC interaction for H4 than observed (250 MHz versus 56 MHz). This discrepancy is about an order of magnitude larger than the typical accuracy, which may be expected from the current level of calculations. For model M4 (O3-centered), a significantly smaller isotropic HFC (roughly 100 MHz) is predicted, but this is still too big, and in addition, the deviation with the experimental g tensor is considerably larger. Model M6 (O2′-centered) has already been assigned to radical species T3 and, in addition, shows no correspondence with the experimental data for both the g and HFC tensor.

Assuming for now that T4 is O4-centered, the Heller−McConnell relationship for the isotropic coupling of a β-proton[47] indicates that either a considerable change (about 40°) in the dihedral angle (D) between the lone electron orbital (LEO) axis and the C4−H4 bond (viewed along the C4−O4 bond) or a strong reduction (by about 75%) of the spin density at O4 is required to obtain a value reconcilable with experiment. The latter is implausible and should be reflected in a much lower g anisotropy. A reorientation by 40° of the LEO, however, must result in larger deviations between calculated and experimental g_{min} and g_{inter} principal directions. This was indeed observed for several variations on model M5 that retain the local radical geometry, including models in which the proton is transferred along hydrogen bonds to surrounding molecules. An example is given in the Supporting Information (Figure S2 and Table S4). DFT calculations were also performed on several broken-ring variations of M5 (allowing for reorientation of the C4−H4 bond, which also results in a different dihedral angle) and alternative conformations of model M4, but few semistable conformations were found, and all of these yielded a considerably worse overall agreement with the experimental data.

In summary, our DFT calculations do not support the assignation by Samskog and Kispert to an H-loss O2′-centered alkoxy, and we tentatively assign T4 to an alkoxy species centered at O4, but no firm structural assignation can be made at present.

4.3.5. Alkoxy Radicals T5 and T6. T5 and T6 each exhibit one big hyperfine interaction (isotropic value around 9 mT ≈ 250 MHz) and a g anisotropy, which is markedly larger than the other alkoxy species (T3, T4, and R3) but within the range of values reported in literature for alkoxy species ($2.021 \leq g_{max} < 2.110$).[48] They correspond to radical species III and IV, respectively, in the 77 K study of Samskog and Kispert[25] (see also (section 4.2.1). These were assigned to an H-loss, O3′-centered radical (model M7 in Figure 10), and a pristine anion,

Table 7. DFT-Calculated Proton HFC Tensors (in MHz) and g Tensors for an H-Loss O3′-Centered Species (M7 in Figure 10)[a]

					principal directions			
radical model	tensor	principal values	isotropic value	anisotropic values	a	b	c	δ (deg)
M7	H(C1′)	39.83	36.09	3.74	−0.242	0.551	−0.799	
		35.69		−0.40	0.323	−0.730	0.602	
		32.75		−3.34	0.915	0.404	−0.002	
	H(C2′)	1.95	−7.28	9.23	−0.577	0.149	0.803	
		−8.00		−0.72	−0.184	−0.982	0.050	
		−15.79		−8.51	0.796	−0.118	0.594	
	H(C3′)	124.26	114.41	9.85	0.653	0.656	−0.379	
		110.32		−4.09	0.696	−0.321	0.643	
		108.64		−5.76	−0.300	0.684	0.665	
	g	2.0401			−0.022	−0.872	0.489	23
		2.0106			0.924	0.169	0.343	45
		2.0035			−0.382	0.459	0.802	51

[a] δ represents the angles between the DFT-calculated and experimental g tensor principal directions of radical T5 (Table 3).

dx.doi.org/10.1021/jp300979g | J. Phys. Chem. A 2012, 116, 3377−3387

respectively, the latter with the excess electron (and unpaired electron density) localized at the O5 ring oxygen.

DFT-calculated HFC tensors and g tensors of model M7 (O3′-centered) are compared with the experimental tensors of T5 in Table 7. The agreement is poor for both g tensor principal values (Δg_{max} underestimated by more than a factor of 2) and directions, and there are large discrepancies with respect to the number and magnitude of the hyperfine interactions (isotropic values of 114 and 36 MHz in the DFT calculations for HFCs to H(C3′) and H(C1′), respectively, versus a single 250 MHz hyperfine splitting observed experimentally). Clearly, the regular O3′-centered alkoxy species is not a valid model for T5.

The model proposed for T6 in ref 25 (a radical model having the unpaired electron localized at the ring oxygen) is speculative, and to our knowledge, such type of radicals has not yet convincingly been identified in saturated carbohydrate compounds. However, our DFT calculations could neither support nor invalidate the proposed model as DFT calculations on these structures were problematic: the excess electron tended to delocalize and spread out over the entire system, typically yielding numerous, (very) small HFCs and a small g anisotropy. All our attempts to obtain a more localized state by deforming structures (such as stretching of the O5−C5 and O5−C1 bonds) failed.

DFT calculations on various other possible (types of) models, including charged species and alkoxy radicals centered at the ring oxygen (broken-ring conformations) or glycosidic oxygen, did not reveal any other suitable model for T5 or T6. Moreover, the relatively large g anisotropy observed for these species was not encountered in any of the calculations. Samskog and Kispert suggested a variation in the hydrogen bonds of the oxygen radical center as an explanation for the variation in g anisotropy: hydrogen bonds to water protons (type I) supposedly yield g_{max} = 2.03−2.06, while hydrogen bonds to hydroxyl protons of sugar molecules (type II) would result in g_{max} = 2.08−2.11.[25] The energy differences between the oxygen 2p orbitals, and therefore the g tensor anisotropy, can indeed depend quite strongly on the chemical environment of an alkoxy radical. DFT calculations on all H-loss alkoxy radicals (those centered at O2, O3, O2, and O6′ are of type I, and those centered at O4, O6, O3′, and O4′ of type II in trehalose) did, however, not show any such correlation and exhibited a considerably more limited variation in g_{max} values than experimentally observed: 2.030−2.046 for type I and 2.032−2.047 for type II. Removal of hydrogen-bond water molecules yields larger g_{max} values, but the relative differences are considerably smaller than the experimental variation. Although DFT calculated g tensor principal values are known to be relatively inaccurate (as commented already in section 4.3.3), it is somewhat surprising that the DFT calculations would not at all reproduce such (pronounced) relative trends. Together with the lack of agreement for the g tensor principal directions, this seems to suggest that the hypothesis of Samskog and Kispert may be erroneous and that radicals with elevated g_{max} values are perhaps another type of oxygen-centered species, e.g., small molecular fragments that have split off from the parent molecule. The strong, relatively isotropic proton HFCs observed experimentally limit the possibilities. It is interesting to note in this context that an $^{\circ}OCH_3$ radical produced by radiation in an $HOCH_3$ lattice environment, exhibits an experimental g_{max} of 2.088[49] although the different chemical environment of the lattice (rather than the different nature of the radical fragment itself) may also explain the elevated g tensor anisotropy. Clearly, a more elaborate and systematic DFT-study (including an in-depth study of the validity of DFT itself in this context) should be undertaken to draw any conclusions in this respect, but this is well beyond the scope of the current work.

5. DISCUSSION AND CONCLUSIONS

Upon X-irradiation at 77 K, or X-irradiation at 10 K and annealing to 77 K, a variety of radicals are formed in trehalose single crystals. These include (i) two species (R2 and R3) that also are present at 10 K after 10 K irradiation, and (ii) seven new species (T1/T1* and T2−T6). R2, R3, T1/T1*, T2, and T3 have convincingly been identified as H-loss species in the current or previous studies: R2, T1/T1*, and T2 are alkyl species centered at C5, C4, and C1′, respectively, and R3 and T3 are alkoxy species centered at O2 and O2′, respectively. T4 appears to be an alkoxy species of the same type as T3 and R3 but could not be identified. For T5 and T6, which have markedly larger g anisotropies, no suitable radical models could be proposed. A preliminary DFT study suggests these are perhaps not of the standard H-loss alkoxy type. At any rate, the dominant alkyl species (T1/T1*) and the dominant alkoxy species (R3) *have* been identified convincingly.

All the alkoxy radicals reported by Samskog et al.[25] (labeled I to IV in their study) are also observed in the present study. Comparison of g tensors and HFC values shows that radical species I, II, III, and IV correspond to T4, R3, T5, and T6, respectively. T3 was reported for the first time in the present study.

A detailed comparison for the alkyl species is more difficult because the corresponding HFC tensors were not reported in the 77 K study of Samskog et al. T1/T1* most likely corresponds to radical VII as they have the same EPR pattern (1:2:1 triplet with a splitting of roughly 3 mT), distinctly different from that of other species present at 77 K. Samskog et al. suggested that VII is also the same alkyl radical as the triplet reported in their 3 K X-irradiation study.[24] The latter most likely corresponds to species R1 obtained after 10 K X-irradiation.[23] Solely on the basis of the EPR spectra, T1/T1* (Radical VII) indeed appears to be the same species as R1. However, the HFC tensors determined from our ENDOR angular variations, together with the DFT calculations, convincingly identify R1 as a C5′-centered species and T1/T1* as a C4-centered species, both resulting from net hydrogen loss. Radicals R2 and VI both are alkyl species characterized by a doublet of doublets in the EPR spectra. The estimated values of the HFCs for radical VI differ significantly (difference of 1−1.5 mT) from those determined for R2, but considering the fact that the more selective and discriminative ENDOR and EIE techniques were not employed in ref 25, it seems possible that an error was made when analyzing the complex and composite EPR spectrum, which is not dominated by the R2 signal. In our opinion, it is therefore reasonable to assume R2 and VI are the same radical species. Finally, alkyl radical T2 is reported for the first time in the present study; no alkyl species with features similar to those of T2 have been reported in ref 25.

It is interesting to note that T2 (C1′-centered) is structurally equivalent to the H-loss, C1-centered species produced in sucrose by X-irradiation at 10 K.[15] Radical models structurally similar to T1/T1* (radical center at the C4′ carbon in a six-membered ring) have also been proposed in other irradiated carbohydrates, e.g., rhamnose[50] and fructose,[16] but has not been observed in sucrose.

dx.doi.org/10.1021/jp300979g | J. Phys. Chem. A 2012, 116, 3377−3387

The variety of alkoxy(-like) species stabilized at 77 K in trehalose is remarkable. This is in sharp contrast to the observation of only one alkoxy radical in sucrose at 10 K,[15] although there is a strong preferential formation of one species (i.e., R3, O2-centered) here as well. A possible explanation for this variety is the presence of lattice water molecules in trehalose, which are likely to provide more efficient pathways for proton migration and, as such, stabilize deprotonated oxygen-centered cations better. R3 is indeed hydrogen-bound to a water molecule in the pristine lattice, as is T3 (O2′-centered), the only other alkoxy species that was identified with (near) certainty.

It is hard to make any firm statements with respect to the radical reactions and/or recombinations associated with the EPR spectral changes upon annealing from 10 to 80 K (Figure 2). Note that four of the radicals observed at 77 K are already present at 10 K: R2, R3, T3, and T6. It would therefore appear that upon annealing from 10 to 77 K, two radical species, R1 and R4 (observed at 10 K[23]), decay and four radical species (T1/T1*, T2, T4, and T5) are formed. There are, however, no straightforward single-step reaction mechanisms connecting R1 or R4 with any of those four newly appearing species. Either more elaborate, multistep reactions take place or R1 and R4 undergo recombination, leading to EPR-silent products. At any rate, there are at least two more species observed at 77 K than at 10 K. There are several possible explanations: first, the trapped electron reported by Samskog et al. after 3 K X-irradiation, may be present at 10 K, in spite of the absence of ENDOR signals, as it was reported to be stable up to 50 K (see section 2).[24] One can also envisage that a low-concentration species escapes detection at 10 K because of, e.g., line broadening or unfavorable overlap of lines, but its successor *is* detected at 77 K. Finally, two species at 77 K may result from a single precursor at 10 K. With the experimental information available at this stage, it is not possible to draw conclusions about radical reactions and radical recombination between 10 and 77 K. Additional experiments, such as the time dependence of the radical concentration measured at intermediate temperatures, would be necessary for this purpose. We are currently investigating the stable radicals created after RT X-irradiation, and the current study, extended with such measurements, will help to devise mechanistic links between those species and the primary radicals.

■ ASSOCIATED CONTENT

Supporting Information

Experimental angular variation of X-band EPR resonance positions in the bc, ac, and ab planes for radical species R3 and T3-T6, and corresponding simulations using the experimental g and HFC values. DFT-optimized structures of two O4-centered alkoxy radical species, one where only the hydrogen at O4 is removed, and one with an additional carbonyl group formation in a neighboring molecule, which affects the hydrogen bonding to the radical center. Comparison of C_α–H_β directions in the pristine molecule with the A_{max} HFC principal directions of HF1(T1), HF1(T1*), HF2(T1), and HF2(T1*). DFT-calculated proton HFC tensors of H-loss radical species centered at C3, C4, C5, and C5′. Comparison of C–O bond directions in the pristine molecule with the g_{max} principal direction of T3 and T4. DFT-calculated proton HFC tensors of the two H-loss radical species centered at O4 shown in Figure S2. This material is available free of charge via the Internet at http://pubs.acs.org.

■ AUTHOR INFORMATION

Corresponding Author

*Tel: +32 9 264 43 52. Fax: +32 9 264 49 96. E-mail: Freddy.Callens@ugent.be.

Notes

The authors declare no competing financial interest.

■ ACKNOWLEDGMENTS

We wish to acknowledge the Research Foundation-Flanders (Belgium) (F.W.O.-Vlaanderen) and COST P15 for financial support concerning the stay at the University of Oslo. M.A.T. is a research assistant and H.D.C. is postdoctoral fellow of the Fund for Scientific Research-Flanders (Belgium) (F.W.O.-Vlaanderena). We are grateful for discussions with Professor Einar Sagstuen and excellent technical support from Mr. Efim Brondz.

■ REFERENCES

(1) Nakajima, T. *Brit. J. Radiol.* **1989**, *62*, 148–153.
(2) Nakajima, T.; Otsuki, T. *Appl. Radiat. Isot.* **1990**, *41*, 359–365.
(3) Nakajima, T. *Appl. Radiat. Isot.* **1995**, *46*, 819–825.
(4) Yordanov, N. D. *Appl. Magn. Reson.* **1994**, *6*, 241–257.
(5) Stachowicz, W.; Strzelczakburlinska, G.; Michalik, J.; Wojtowicz, A.; Dziedzicgoclawska, A.; Ostrowski, K. *J. Sci. Food Agric.* **1992**, *58*, 407–415.
(6) Diehl, J. F. *Safety of Irradiated Food*; Marcel Dekker: New York, 1995.
(7) Desrosiers, M. F.; Burlinska, G.; Kuppusamy, P.; Zweier, J.; Yaczko, D. M.; Auteri, F. P.; Mcclelland, M. R.; Dick, C. E.; Mclaughlin, W. L. *Radiat. Phys. Chem.* **1995**, *46*, 1181–1184.
(8) Bernhard, W. A.; Close, M. D. *DNA Damage Dictates the Biological Consequences of Ionizing Irradiation: The Chemical Pathways*; Marcel Dekker: New York, 2004.
(9) Becker, D.; Adhikary, A.; Sevilla, M. D. *Charge Migration in DNA: Perspectives from Physics, Chemistry and Biology*; Springer: New York, 2007.
(10) Close, D. M. *Radiat. Res.* **1997**, *147*, 663–673.
(11) Debije, M. G.; Bernhard, W. A. *Radiat. Res.* **2001**, *155*, 687–692.
(12) Weiland, B.; Huttermann, J. *Int. J. Radiat. Biol.* **1998**, *74*, 341–358.
(13) De Cooman, H.; Pauwels, E.; Vrielinck, H.; Sagstuen, E.; Callens, F.; Waroquier, M. *J. Phys. Chem. B* **2008**, *112*, 7298–7307.
(14) De Cooman, H.; Pauwels, E.; Vrielinck, H.; Sagstuen, E.; Van Doorslaer, S.; Callens, F.; Waroquier, M. *Phys. Chem. Chem. Phys.* **2009**, *11*, 1105–1114.
(15) De Cooman, H.; Pauwels, E.; Vrielinck, H.; Sagstuen, E.; Waroquier, M.; Callens, F. *J. Phys. Chem. B* **2010**, *114*, 666–674.
(16) Tarpan, M.; Sagstuen, E.; Pauwels, E.; Vrielinck, H.; Waroquier, M.; Callens, F. *J. Phys. Chem. A* **2008**, *112*, 3898–3905.
(17) Tarpan, M. A.; Pauwels, E.; Vrielinck, H.; Waroquier, M.; Callens, F. *J. Phys. Chem. A* **2010**, *114*, 12417–12426.
(18) Pauwels, E.; Verstraelen, T.; Waroquier, M. *Spectrochim. Acta, Part A* **2008**, *69*, 1388–1394.
(19) Pauwels, E.; Declerck, R.; Van Speybroeck, V.; Waroquier, M. *Radiat. Res.* **2008**, *169*, 8–18.
(20) Pauwels, E.; Van Speybroeck, V.; Waroquier, M. *J. Phys. Chem. A* **2006**, *110*, 6504–6513.
(21) De Cooman, H.; Vanhaelewyn, G.; Pauwels, E.; Sagstuen, E.; Waroquier, M.; Callens, F. *J. Phys. Chem. B* **2008**, *112*, 15045–15053.
(22) Pauwels, E.; De Cooman, H.; Vanhaelewyn, G.; Sagstuen, E.; Callens, F.; Waroquier, M. *J. Phys. Chem. B* **2008**, *112*, 15054–15063.
(23) Tarpan, M. A.; De Cooman, H.; Sagstuen, E.; Waroquier, M.; Callens, F. *Phys. Chem. Chem. Phys.* **2011**, *13*, 11294–11302.
(24) Samskog, P. O.; Kispert, L. D.; Lund, A. *J. Chem. Phys.* **1983**, *78*, 5790–5794.

(25) Samskog, P. O.; Kispert, L. D. *J. Chem. Phys.* **1982**, *77*, 2330−3335.
(26) Sagstuen, E.; Lund, A.; Awadelkarim, O.; Lindgren, M.; Westerling, J. *J. Phys. Chem.* **1986**, *90*, 5584−5588.
(27) Brown, G. M.; Rohrer, D. C.; Berking, B.; Beevers, C. A.; Gould, R. O.; Simpson, R. *Acta Crystallogr., Sect. B: Struct. Sci.* **1972**, *28*, 3145−3158.
(28) Nelson, W. H. *J. Magn. Reson.* **1980**, *38*, 71−78.
(29) Schonland, D. S. *Proc. Phys. Soc.* **1959**, *73*, 788−792.
(30) Vrielinck, H.; De Cooman, H.; Tarpan, M. A.; Sagstuen, E.; Waroquier, M.; Callers, F. *J. Magn. Reson.* **2008**, *195*, 196−205.
(31) Stoll, S.; Schweiger, A. *J. Magn. Reson.* **2006**, *178*, 42−55.
(32) Becke, A. D. *Phys. Rev. A* **1988**, *38*, 3098−3100.
(33) Lee, C. T.; Yang, W. T.; Parr, R. G. *Phys. Rev. B* **1988**, *37*, 785−789.
(34) http://cp2k.berlios.de.
(35) Declerck, R.; Van Speybroeck, V.; Waroquier, M. *Phys. Rev. B* **2006**, *73*, 115113−115121.
(36) Weber, V.; Iannuzzi, M.; Giani, S.; Hutter, J.; Declerck, R.; Waroquier, M. *J. Chem. Phys.* **2009**, *131*, 014106−014117.
(37) Lippert, G. H. J.; Parrinello, M. *Theor. Chem. Acc.* **1999**, *103*, 124−140.
(38) Lippert, G.; Hutter, J.; Parrinello, M. *Mol. Phys.* **1997**, *92*, 477−487.
(39) Lippert, G.; Hutter, J.; Ballone, P.; Parrinello, M. *J. Phys. Chem.* **1996**, *100*, 6231−6235.
(40) Goedecker, S.; Teter, M.; Hutter, J. *Phys. Rev. B* **1996**, *54*, 1703−1710.
(41) Hartwigsen, C.; Goedecker, S.; Hutter, J. *Phys. Rev. B* **1998**, *58*, 3641−3662.
(42) Box, H. C.; Budzinski, E. E.; Potienko, G. *J. Chem. Phys.* **1978**, *69*, 1966−1973.
(43) Box, H. C.; Budzinski, E. E.; Potienko, G. *J. Chem. Phys.* **1980**, *73*, 2052−2056.
(44) Vanhaelewyn, G.; Lahorte, P.; De Proft, F.; Mondelaers, W.; Geerlings, P.; Callens, F. *Phys. Chem. Chem. Phys.* **2001**, *3*, 1729−1735.
(45) Improta, R.; Barone, V. *Chem. Rev.* **2004**, *104*, 1231−1253.
(46) Budzinski, E. E.; Box, H. C. *J. Chem. Phys.* **1985**, *82*, 3487−3490.
(47) Bernhard, W. A.; Close, D. M.; Hüttermann, J.; Zehner, H. J. *Chem. Phys.* **1977**, *67*, 1211−1219.
(48) Box, H. C.; Budzinski, E. E.; Freund, H. G. *J. Chem. Phys.* **1984**, *81*, 4898−4902.
(49) Gerson, F.; Huber, W. *Electron Spin Resonance Spectroscopy of Organic Radicals*; Wiley-VCH: Weinheim, Germany, 2003.
(50) Sagstuen, E.; Lindgren, M.; Lund, A. *Radiat. Res.* **1991**, *128*, 235−242.